Predictive capabilities of corotating interaction regions using STEREO and Wind in-situ observations

Chi, Y., Shen, C., Scott, C. ORCID: https://orcid.org/0000-0001-6411-5649, Xu, M., Owens, M. ORCID: https://orcid.org/0000-0003-2061-2453, Wang, Y. and Lockwood, M. ORCID: https://orcid.org/0000-0002-7397-2172 (2022) Predictive capabilities of corotating interaction regions using STEREO and Wind in-situ observations. Space Weather, 20 (7). e2022SW003112. ISSN 1542-7390 doi: 10.1029/2022SW003112 Available at https://centaur.reading.ac.uk/105723/

Space Weather®

RESEARCH ARTICLE
10.1029/2022SW003112

Predictive Capabilities of Corotating Interaction Regions Using STEREO and *Wind* In-Situ Observations

Yutian Chi[1,2], Chenglong Shen[1,2], Christopher Scott[3], Mengjiao Xu[1,4], Mathew Owens[3], Yuming Wang[1], and Mike Lockwood[3]

[1]CAS Key Laboratory of Geospace Environment, Department of Geophysics and Planetary Sciences, University of Science and Technology of China, Hefei, China, [2]CAS Center for Excellence in Comparative Planetology, University of Science and Technology of China, Hefei, China, [3]Department of Meteorology, University of Reading, Reading, UK, [4]Anhui Mengcheng Geophysics National Observation and Research Station, University of Science and Technology of China, Mengcheng, China

Key Points:

- Spacecraft longitudinal and latitudinal separation can significantly affect the accurate forecast of Corotating Interaction Regions (CIRs)
- More than 93.2% of CIRs can be reliably predicted in advance with separations of less than 30° longitude and ±5° latitude
- Most of CIRs arrived at Earth earlier than predicted, when Solar Terrestrial Relations Observatory-B was located to the south of the Earth in the Heliocentric Earth Equatorial coordinate

Correspondence to:
C. Shen,
clshen@ustc.edu.cn

Citation:
Chi, Y., Shen, C., Scott, C., Xu, M., Owens, M., Wang, Y., & Lockwood, M. (2022). Predictive capabilities of corotating interaction regions using STEREO and *Wind* in-situ observations. *Space Weather*, *20*, e2022SW003112. https://doi.org/10.1029/2022SW003112

Received 5 APR 2022
Accepted 16 JUN 2022

Author Contributions:
Supervision: Chenglong Shen
Writing – original draft: Yutian Chi

Abstract Solar wind stream interaction regions (SIRs) and corotating interaction regions (CIRs) can cause geomagnetic storms and change energetic particle environment, ionospheric composition on Earth. Therefore advanced warning of SIRs/CIRs is vital for mitigating the effect of space weather on critical infrastructures in modern society. Recently, several solar missions, for example, Vigil mission (Luntama et al., 2020) and Solar Ring mission (Wang et al., 2020), that can be served as a space weather monitor, have been proposed. To evaluate the capabilities of these future missions of predicting SIRs/CIRs, the Solar Terrestrial Relations Observatory (STEREO-B) spacecraft is used to investigate the correlation between SIRs/CIRs detected by STEREO-B and *Wind* spacecraft. The correlation coefficients of solar wind velocity in SIRs/CIRs are significantly higher than that of magnetic field intensity or plasma density. It indicates that the velocity structure of solar wind is more persistent than magnetic field and ion density. By assuming the SIR/CIR structures are stable and ideal corotation, 58.9% of SIRs/CIRs in the STEREO-B CIR catalog can be used to predict CIR arrival time in near-Earth space. With increasing longitudinal and latitudinal separations between STEREO-B and *Wind*, the percentage of accurately predicted CIRs decreases gradually from 100% to 20%. If the separation angle between STEREO-B and *Wind* is within 30° in longitude and approximately ±5° in latitude, more than 93.2% of SIRs/CIRs can be accurately predicted several days in advance. This demonstrates that a spacecraft situated 30° trailing Earth in its orbit, can optimize our space weather-predicting capabilities for the Earth and lessen the risk of missing or "false alarms" CIRs.

Plain Language Summary Stream interaction regions (SIRs) are formed by the interactions between the fast solar wind streams originating from coronal holes and slow solar wind streams. SIRs can corotate with the sun and they can also be called as Corotating Interaction Regions (CIRs), if those structures recur on successive solar rotations. When SIRs/CIRs reach the Earth, they may cause recurrent geomagnetic storms, alter the energetic particle environment around the Earth, and other meteorological processes in Earth's lower atmosphere, posing a threat to satellite systems, radio communications, electrical transmission, and technological critical infrastructure. As a result, the analysis and forecast of when SIRs/CIRs will hit the Earth is a critical issue in the space weather community. This study investigates the prediction ability of SIRs/CIRs with varied longitudinal and latitudinal spacecraft separations using in-situ measurements from the Solar Terrestrial Relations Observatory (STEREO-B) and *Wind* spacecraft. The statistical results reveal that the spacecraft longitudinal and latitudinal separation can have a significant impact on the accuracy of the SIRs/CIRs forecast. According to STEREO-B in-situ data, when the latitudinal separation is less than ±5° and the longitudinal separation is less than 30°, more than 93.2% CIR events can be well predicted in advance.

1. Introduction

Hazardous space weather endangers Earth's geomagnetic environment, causes geomagnetic storms, and poses a threat to satellite systems, radio communications, electrical transmission, and technological critical infrastructure (Cannon et al., 2013; Hapgood, 2011). As people become more reliant on modern technology, predicting space weather is becoming more important. Stream Interaction Regions (SIRs) are solar wind structures formed between the fast solar wind stream originating from coronal holes and the high-density, low-speed wind from the streamer belt. The SIRs are also referred as Corotating Interaction Regions (CIRs, [Gosling & Pizzo, 1999]) when they recur on successive solar rotations. CIRs are the main sources of moderate and minor recurrent geomagnetic

storms (Chi et al., 2018; Echer et al., 2013; Gosling & Pizzo, 1999; Jian et al., 2006; Vršnak et al., 2017). If they reach down to the heliographic latitude of Earth, they sweep over the Earth once per solar rotation and cause a sequence of effects with a roughly 27-day periodicity. These effects include recurrent geomagnetic storms (Chi et al., 2018; Echer et al., 2013; Jian et al., 2006), changes in the energetic particle environment on Earth (Rouillard & Lockwood, 2007), in the ionosphere (Yu et al., 2021), in the occurrence of lightning (C. J. Scott et al., 2014), and other meteorological processes in Earth's lower atmosphere (Harrison & Lockwood, 2020). In rare cases, CIRs can also cause intense geomagnetic storms (Chi et al., 2018; Gonzalez et al., 2011). CIRs are used throughout the rest of this article to refer to the interaction between rapid and slow solar wind, assuming that all events are stable and ideally corotation, regardless of whether they recur more than one solar rotation.

As CIRs recur with the Sun's equatorial rotation every 27 days, M. J. Owens et al. (2013) used the 27 days persistence model to forecast the near-Earth solar wind conditions, which is comparable to numerical models during solar minimum. Miyake et al. (2005) found the correlation of solar wind between the Nozomi spacecraft located at the L5 point and ACE is significantly higher than the 27-day recurrence of ACE data. Thus, it is expected that observations from solar wind monitor trailing Earth in its orbit will provide an early warning of CIRs approaching at Earth and causing hazardous space weather. Several future space weather mission concepts have been proposed as a probe located behind the Earth, such as the Vigil mission located around the L5 point proposed by the European Space Agency (ESA) (Luntama et al., 2020) and the Solar Ring Mission with 30° and 150° trailing Earth in its orbit proposed by Wang et al. (2020). The twin Solar Terrestrial Relations Observatory (STEREO) spacecraft (Kaiser et al., 2008), which launched in 2006 and orbited the Sun in the ecliptic plane, drifting away from the Earth at a rate of around 22.5° per year, can be used as pathfinders for the future space weather monitoring mission. Using the observations from STEREO-A, STEREO-B, and *Wind*, several studies have been conducted to determine if the L5 point is a particularly beneficial site for space weather forecast and monitoring, including: solar wind condition prediction (Barnard et al., 2022; Simunac, Kistler, Galvin, Lee et al., 2009, Simunac, Kistler, Galvin, Popecki, & Farrugia, 2009; Thomas et al., 2018); comprehensive understanding of Coronal Mass Ejections (CMEs) propagation (C. Scott et al., 2019; Rodriguez et al., 2020); prediction of the geomagnetic storms (Bailey et al., 2020). Most of these studies compared observations from two in-situ observers separated by 60° and were limited to only a few months of data. Allen et al. (2020) compared CIR catalogs at STEREOA/B (Jian et al., 2019) and *Wind* (Chi et al., 2018; Jian et al., 2006) to investigate probability of repeat detection of CIRs at various longitudinal separations. However, fewer works have tried to investigate how accurately the CIRs can be predicted and what factors may influence the rotation speed of CIRs.

This study focuses on observations by STEREO-B, which trailing Earth in its orbit, to perform a logical test for forecasting CIRs for the future solar wind monitors, particularly for the Solar Ring Mission (Wang et al., 2020). To compare with STEREO-B, in-situ observations from *Wind* spacecraft, which is located around the L1 point, are also used in this study. The differences in heliographic longitude between STEREO-B and *Wind* increased from 0.2° to 165° since the launch of STEREO-B until its loss at the end of 2014, while the latitudinal separations show an annual variation with an amplitude that increased with the longitude separation, reaching a maximum value of −15° to 15° in 2014. It should be noted that as longitude and latitude increase, solar activity transits from solar minimum to maximum, making the isolation of a single factor that affects the predictive capabilities of CIRs more challenging (Turner et al., 2021). The magnetic field intensity, solar wind bulk velocity, and ion density are the three key solar wind parameters, which are used in empirical models (Temerin & Li, 2002; Wang et al., 2003) to predict the corresponding geomagnetic storm's intensity (Dst index). By calculating the summed correlation coefficient for three key solar wind parameters of CIRs between time-shifted STEREO-B and *Wind* in-situ data, we investigate the percentage of CIRs that can be accurately predicted at various longitudinal and latitudinal separations. The layout of the paper is as follows. Section 2 presents the CIR data sets and methods used in this study. The results of this analysis are given in Section 3, while the discussion and summary of the findings are presented in Section 4.

2. Data and Analysis

CIRs are characterized by in-situ observations according to the criteria of a distinct rise in solar wind velocity, an enhancement in the magnetic field intensity, a first increase and subsequently a fall in proton density, an increase in proton temperature, and a maximum of total pressure at the stream interface (Chi et al., 2018; Jian et al., 2006, 2011). Based on those criteria, two CIR catalogs have been established using the *Wind* and Advance

Composition Explorer (ACE) in-situ observations around L1 and STEREO-A/B in-situ observations, respectively. The CIRs catalog at the L1 point was established by Jian et al. (2006) during the period 1995–2004, and then was extended to the end of 2016 by Chi et al. (2018) using the same criteria. Jian et al. (2019) also produced another CIR event list based on the STEREO-A/B in-situ observations from 2007 to 2016. Using the two catalogs, we investigate how well the STEREO-B in-situ data can be used to predict the arrival time of CIRs at Earth at various longitudinal and latitudinal angles.

During 2007–2014, 257 CIR events have been identified by STEREO-B (Jian et al., 2019), while 244 CIR events have been identified by *Wind* spacecraft (Chi et al., 2018; Jian et al., 2006). Some CIR events have been found to interact with CMEs during their propagation from the Sun to Earth (Chi et al., 2018). CMEs are transitory phenomena characterized by enhanced magnetic field intensity and velocity. They are more likely to be detected by a single spacecraft and do not impact two observers with a time lag derived from their longitudinal separation. CIR-ICME interactions may affect the CIRs' in-situ characteristics, reducing the correlation coefficients of solar wind parameters for the same CIR event recorded by *Wind* and STEREO-B. Thus, 5 CIR-ICME interaction events detected by *Wind* are excluded from this analysis, according to the CIR-ICME interaction catalog from Chi et al. (2018) and the ICME catalog from Chi et al. (2016). For the CIRs observed by STEREO-B, according to the ICME catalog from Jian et al. (2018), 3 CIR-ICME interaction events were excluded from this analysis. In addition, the CIR events with a data gap may also influence the correlation coefficients between the two spacecraft and need to be removed. After carefully eliminating CIRs interacted with ICMEs or with data gaps, we arrived at a list of 219 CIRs at STEREO-B and 216 CIRs at *Wind*.

By assuming the CIR structures are steady and ideally co-rotating with the Sun, the characteristics of CIRs detected at STEREO-B are expected to be observed at L1 with appropriate time-shifting. The benchmark time lag (ΔT_{ben}) between the two spacecraft can be calculated by accounting for the longitudinal separation angle between the two spacecraft and the differences in radial position. The CIRs' rotation period (T_{cir}) is assumed to be 27.13 days according to M. J. Owens et al. (2013), slightly faster than the solar rotation speed at the solar equator. The temporal separation results from the radial positions of the two spacecraft can also be estimated by assuming solar wind bulk velocity as a constant over this short radial distance. In this work, we use the same method from Vennerstrom et al. (2003) and Opitz et al. (2009) to estimate the temporal separation. Thus, the basic equation to calculate the benchmark time lag is shown as Equation 1 as following,

$$\Delta T_{ben} = \frac{\Delta\Phi_{STB}}{\Omega_{sun}} + \frac{R_{Earth} - R_{STB}}{V} \tag{1}$$

$\Delta\Phi_{STB}$ is the longitudinal separation between STEREO-B and Earth in Heliocentric Earth Equatorial (HEEQ) coordinate. Ω_{sun} is the angular rotation velocity of CIRs at the solar equator ($360°/T_{cir}$). V is the maximum solar wind bulk velocity of the CIR detected by STEREO-B. $R_{Earth} - R_{STB}$ is the difference between the two spacecraft at the radial position. Based on Equation 1, the benchmark lagged time can be estimated from the positions of the two spacecraft.

The solar wind conditions detected at STEREO-B are used to forecast the solar wind characteristics at Earth under two fundamental assumptions: ideal corotation of CIRs and negligible evolution of the solar wind source during the time of CIRs rotating from STEREO-B to Earth. The actual lag time of the CIRs may differ from the benchmark lag time due to the evolution of the source region (coronal hole) (Simunac, Kistler, Galvin, Popecki, & Farrugia, 2009), and the latitudinal differences (M. Owens et al., 2019). As a result, a time range of ±30 hrs around the benchmark lag time is appropriate for searching the related CIRs detected by *Wind* and STEREO-B. It should be noted that the limited search time range may cause some CIRs to be overlooked, especially for large longitudinal separations. We determine the actual lag time of CIR events at Earth by maximizing the summed correlation coefficient between the three key parameters measurements at STEREO-B and *Wind* in-situ observations. According to the start and end time of CIR detected from the STEREO-B, the majority of CIR events span less than 3 days at one in-situ observer. Therefore, we use a 3-day time window from the start of the CIR to calculate the maximum time-shifted summed correlation coefficients between STEREO-B and *Wind* measurements. The time resolution of all spacecraft data used in this analysis is 10 min. Figure 1 shows the comparison of *Wind* and time-shifted STEREO-B for magnetic field intensity ($|B|$), solar wind bulk speed (V_{sw}), and proton temperature (T_p) from April 27 to 3 May 2010. During that time, the STEREO-B and Earth are separated by 70.95° in HEEQ longitude and by 0.003AU in radial. According to Equation 1, the benchmark lag time is 129.22 hr.

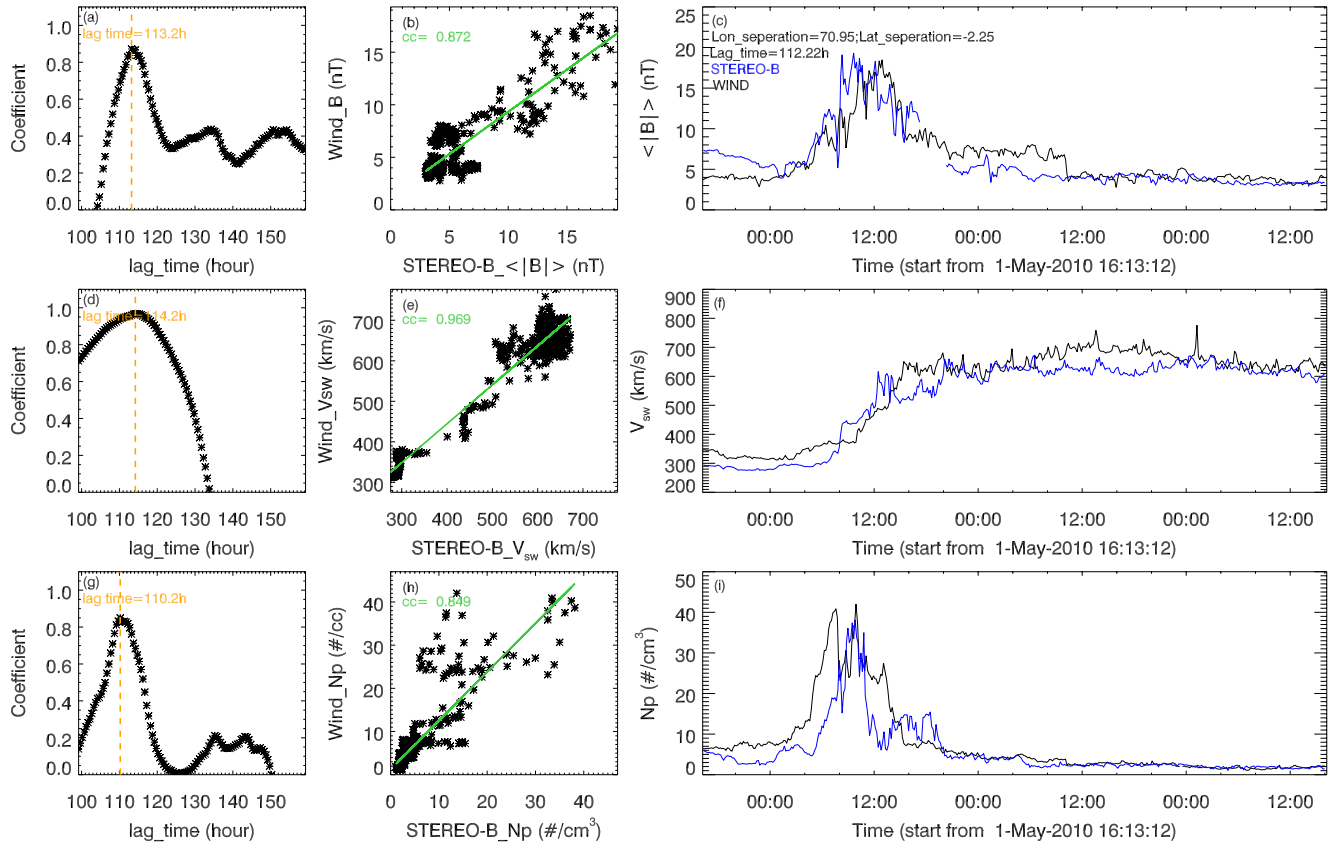

Figure 1. Plots for the corotating interaction region event detected by *Wind* on May 1–3, 2010. The left column shows the correlation between *Wind* and time-shifted Solar Terrestrial Relations Observatory (STEREO-B) magnetic field, velocity, and proton density data using a time window of [−30, 30] hours around the calculated benchmark time delay. The dashed orange vertical lines show the corrected lag time at the highest correlation coefficient. Regression plots of *Wind* and time-shifted STEREO-B magnetic field, velocity, and proton density data at the maximum correlation coefficient are plotted in the middle column. The green lines represent the linear regression between *Wind* and time-shifted STEREO-B data. The right column shows a comparison between *Wind* and time-shifted STEREO-B data, including the magnetic field, velocity, and proton density at corrected lag time. The black lines represent parameters detected by *Wind*, while the blue lines represent parameters detected by STEREO-B with a time shift of 112.34 hr.

Correlation coefficients between the time-shifted STEREO-B and *Wind* were calculated and plotted against time lag, as shown in Figure 1 panels a, d, and g. The dashed orange vertical lines show the lag time at the peak correlation coefficient: 113.2 hr for the magnetic field, 114.2 hr for velocity, and 110.2 hr for plasma density. The lag time at the highest correlation coefficient is 15 hr earlier than expected, indicating that this CIR event recurred faster than expected. The panels b, e, and h show the regression plot of *Wind* and time-shifted STEREO-B for magnetic field, velocity, and proton density data at the highest correlation coefficient. The observed parameters at *Wind* and time-shifted STEREO-B display an excellent correlation. The green lines in those panels present a linear fit for each parameter. The peak correlation coefficients between time-shifted STEREO-B and *Wind* for the magnetic field, velocity, and plasma density are 0.872, 0.969, and 0.849, respectively.

The peak correlation coefficients for the three parameters are at different lag times. Therefore, the corrected lag time at the maximum summed correlation coefficient (the sum of all the coefficients for the three key parameters) is used to find the corresponding CIR events detected by the *Wind* spacecraft. When the summed correlation coefficient was greater than 1.8, we expect the large-scale CIR structure to remain mainly intact as it moves from STEREO-B to Earth. Figures 1c, 1f, and 1i show the overlay of the observations from *Wind* and time-shifted STEREO-B when the summed correlation coefficient between them is at its maximum. The black lines in panels c, f, and i show the *Wind* in-situ observations for magnetic field intensity, solar wind bulk velocity, and ion density, while the blue lines show the time-shifted (112.22 hr) STEREO-B in-situ observations. The longitude and latitude separations in HEEQ coordinates, as well as the actual temporal separation between STEREO-B and *Wind*, are presented in Panel c. STEREO-B is located south of the Earth when the latitudinal

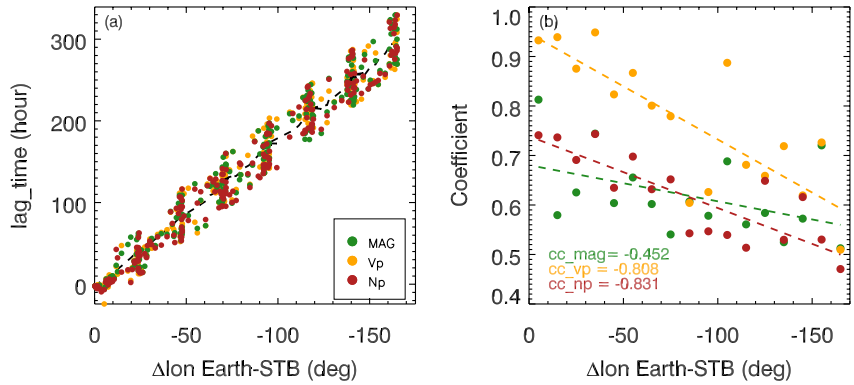

Figure 2. Panel a compares the time lag at the maximum total correlation coefficients to the longitude separation for all corotating interaction region events. The dashed black line represents the benchmark lag time based on the relative positions of the Solar Terrestrial Relations Observatory-B and *Wind* spacecraft. Panel b shows the correlation coefficients for the magnetic field, velocity, and plasma density as a function of spacecraft separation angle.

separation angle is negative. The trends in the magnetic field intensity and velocity profiles recorded at Earth in Figures 1c and 1f are remarkably similar to the time-shifted STEREO-B data, in spite of the longitude separation between the two observers being larger than 70°. Even though the trends in the measured plasma density agree with STEREO-B forecasts, there is an offset at the peak of plasma density. Due to the considerable longitudinal separation (70.95°), *Wind* and STEREO-B would have detected different parcels of plasma originating from the same, potentially evolving, coronal hole. Therefore, in addition to the evolution of CIR compression regions (Simunac, Kistler, Galvin, Lee, et al., 2009), the source evolution should be dominantly responsible for the offset of the peak of plasma density.

3. Observations

Using the same method, we analyze 219 CIR events detected by STEREO-B. Figure 2 shows the distribution of the lag time at the peak correlation coefficient versus the longitudinal separation angle between STEREO-B and *Wind* spacecraft. The black line in panel a shows the benchmark lag time according to the longitudinal and radial separation. The green, orange, and red points in Figure 2 represent the actual lag time for the magnetic field, velocity, and plasma density, respectively. Panel b shows the correlation coefficient of the three parameters versus the longitudinal separation. The correlation coefficients for solar wind velocity are substantially greater than those for magnetic field or plasma density, as shown in Figure 2b. It confirms that the velocity of solar wind is more persistent than magnetic field and plasma density (Simunac, Kistler, Galvin, Lee, et al., 2009). The dashed lines in Panel b are the linear fit for the longitudinal separation and the correlation coefficient. As the longitudinal separation angle increases, the correlations of the magnetic field intensity, solar wind bulk velocity, and ion density drop rapidly, implying that the CIR events evolve more significantly with a larger separation angle between the two observers.

As shown in Figure 2a, there are disparities between the benchmark lag time and the actual lag time for the majority of CIR events. Even at a similar longitudinal separation angle, the actual lag time for different CIR events can differ by many hours. The lag time bias is used to express the differences between the actual lag time and the benchmark lag time, which can be explained by the evolution of the coronal hole, radial velocity or the latitudinal separation. As a result, the impact of the maximum bulk velocity and the latitudinal separation between the two observers on the lag time bias will be discussed further below.

Because of the development, diminishing, or disappearance of the coronal hole, some CIR events in the STEREO-B CIR catalog cannot be identified at Earth, showing a poor correlation coefficient between time-shifted STEREO-B and *Wind* in-situ observations. As we mentioned before, when the total correlation coefficient is greater than 1.8, we expect that the CIR event can be accurately predicted by the STEREO-B spacecraft, which trailed Earth in its orbit. As shown in Table 1, 129 (58.9%) CIRs can be accurately predicted. Figure 3 shows the relationship between the lag time bias and the maximum velocity detected at STEREO-B for the CIRs with a summed correlation coefficient larger than 1.8. Lag time biases are the differences between the benchmark lag time and the

Table 1
A Comparison of Corotating Interaction Regions (CIRs) Detected by Wind and Time-Shifted Solar Terrestrial Relations Observatory (STEREO) From 2007 to 2014

—	STEREO-B	Wind
Total events	219	216
Accurately predicted events[a]	129 (58.9%)	129 (59.7%)
Bad predicted events[b]	26 (11.9%)	26 (12.0%)
Misses[c]	—	61 (28.2%)
False alarms[d]	64 (29.2%)	—

[a]"Accurately predicted events" indicate the number of CIRs from two CIR catalogs with the summed correlation coefficient larger than 1.8. [b]"Bad predicted events" are CIRs in both data sets but the summed correlation coefficient for the three parameters is less than 1.8. [c]"Misses" are CIRs only detected by *Wind*. [d]"False alarms" are CIRs only appear in STEREO-B in-situ observations.

lag time at the maximum summed correlation coefficient. Positive lag time bias values suggest that CIRs arrive at Earth earlier than predicted, while negative values indicate that CIRs arrive later than expected. The average lag time biases for the magnetic field, velocity, and plasma density are shown in green, orange, and red dot symbols, respectively, in each 60 kms^{-1} velocity interval. The black circles show the differences between the benchmark arrival time and the actual arrival time of CIRs (corrected time bias) at *Wind*. The black dashed line shows the best linear fit between the corrected lag time bias and maximum velocity detected at STEREO-B. The correlation coefficient between them is −0.702, suggesting that the higher the bulk velocity of CIRs detected by STEREO-B, they are likely to reach Earth sooner than predicted. Figure 3b shows a histogram of the maximum velocity of CIRs detected by STEREO-B. The majority of maximum velocities are in the range of 550–700 kms^{-1}. Due to the rare number of events with a maximum velocity greater than 800 kms^{-1}, a higher inaccuracy in the average lag time bias might induce for the CIRs with higher velocities. Thus, when predicting the arrival time of CIRs at Earth, the maximum velocity detected by the preceding spacecraft must be taken into account.

Both radial and longitudinal separations between the two observers are taken into consideration when determining the benchmark lag time, but the effects of the latitude separation are ignored. In practice, the monitoring spacecraft and the targeted prediction site are usually separated by a latitudinal offset (M. Owens et al., 2019). If a coronal hole border has a different longitude at various latitudes, the spacecraft at different latitudes will encounter the CIR at different times, resulting in a bias in lag time. Figure 4 presents the lag time bias as a function of the latitudinal separation between *Wind* and STEREO-B. The gray plus symbols show the corrected lag time bias for all the CIR events. The green, yellow, and red points present average lag time bias for each 2.5° longitudinal separation for magnetic field, velocity, and plasma density, respectively. The black circles indicate the corrected lag time bias, and the black dashed line in Figure 4 is the best linear fit for the corrected lag time bias. Negative Δ lat values indicate STEREO-B is located at the south of the Earth, and vice versa. As shown in Figure 4, when the Δ lat is negative, most of the lag time bias values are negative, which means that the CIRs have a strong bias to arrive at the Earth earlier than expected. It is consistent with the rotation rates of coronal holes in the southern hemisphere are slightly higher than those in the northern hemisphere (Bagashvili et al., 2017). As shown in Bagashvili et al. (2017), the rotation rates of coronal holes are associated with their latitude position and area. More study is needed in the future to investigate the effects of the two spacecraft's relative latitudinal positions.

The distribution of the CIRs with the longitudinal and latitudinal separation between STEREO-B and *Wind* spacecraft are shown in Figure 5. The colorbar for Figure 5a indicates the summed correlation coefficient of CIRs

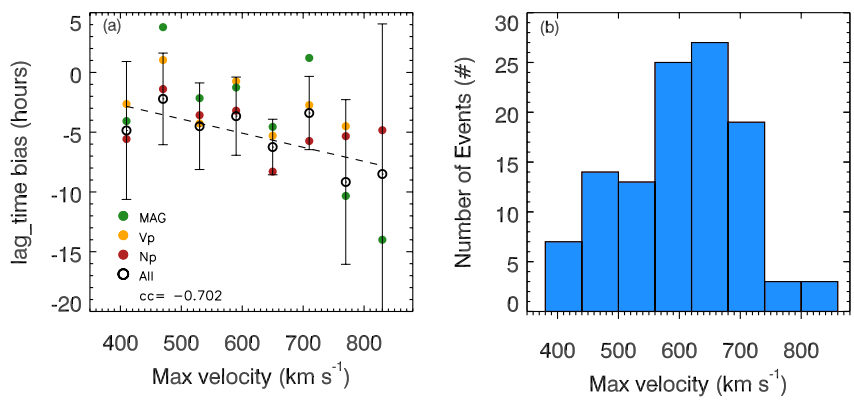

Figure 3. Panel (a) shows the relationship between the lag time bias and the peak velocity of the corotating interaction regions detected at Solar Terrestrial Relations Observatory (STEREO). Panel (b) presents a histogram of maximum solar wind velocity detected by STEREO-B spacecraft at a 10-min resolution. Standard errors are calculated as $\sigma/\sqrt{N}$ for each group.

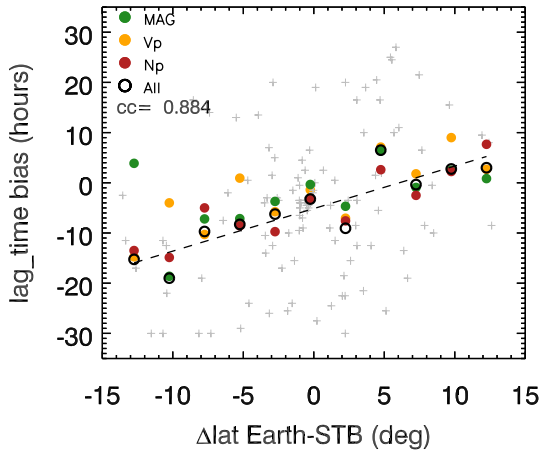

Figure 4. The relationship between the lag time bias and Δlat. The average lag time bias for different separation latitudes of the magnetic field, velocity, and plasma density is represented by the green, yellow, and red circles, respectively. The gray plus symbols present the best lag time bias for all the well-predicted corotating interaction region events, and the black circles show the average lag time bias for each 2.5°.

between time-shifted STEREO-B and *Wind* spacecraft. When the correlation is weak, the color of the points tends to be green, and when the correlation is strong, the color of the points tends to be reddish. As shown in Figure 5a CIRs with stronger correlations are localized at longitudinal separations less than 50° and latitudinal separations less than 5°. The rising longitudinal separations, combined with increased solar activity, may easily break down the steady-state assumption of CIRs, resulting in a higher forecast inaccuracy (Turner et al., 2021). Panels b and c show the histograms of longitudinal and latitudinal separation angle between STEREO-B and *Wind* spacecraft, respectively. Dark blue and light blue bars represent the numbers for all CIR events and well predicted CIR events (summed correlation coefficient greater than 1.8), while the blue asterisks display the ratio between them. As seen in panel b, the percentage of accurately predicted CIR events decreases with longitudinal separation, which is consistent with the findings from Allen et al. (2020). The longitudinal separation between 100° and 110° is an exception, because only 2 CIR events are recorded during that interval. STEREO-B can accurately forecast CIRs to a degree of greater than 65% when the separation angle is smaller than 50°, which is comparable to the likelihood of repeated CIRs (74.6%) at L5 point from (Allen et al., 2020). When the longitudinal separation angle is more than 40°, there is a considerable increase in false alarms. According to Wang et al. (2020), the future solar wind monitor is proposed to be located 30° trailing Earth in its orbit, which is hopefully capable of accurately predicting more than 93.2% of CIRs.

As the higher latitudinal separation between *WIND* and STEREO-B spacecraft occurred only when the longitudinal separation was large, we rule out the skew induced by another factor, while evaluating the accuracy of predicted CIR affected by individual longitudinal or latitudinal separation. In order to investigate the effect of the accuracy of forecasting CIR characteristics from the longitudinal separations, Figure 6a displays the histograms of longitudinal separation angle and the percentage of accurately predicted CIRs with absolute latitude separations less than 5°. As shown in Figure 6a, there is a clear decrease in the percentage of accurately predicted CIR events with longitudinal separation. Figure 6b shows the histograms of latitudinal separation and the percentage of accurately predicted for the CIRs with longitudinal separations larger than 90°. The numbers of identified CIRs events do not show a significant dependence on latitude. The latitudinal separation between the spacecraft had no significant effect on the probability of recurring CIR detection (Allen et al., 2020), but the chances of accurate prediction of CIRs characteristics at Earth fall fast as absolute latitudinal separation grows. It confirms that the latitudinal separation between two observers is the key factor that influences the accuracy of forecasting CIR characteristics (M. Owens et al., 2019).

However, several CIR events can still be reliably predicted by STEREO-B with longitudinal separation wider than 130°. For example, the blue circle in Figure 5 panel (a) presents a CIR event identified by the STEREO-B spacecraft from November 26–29, 2013, and by *Wind* spacecraft from December 7–10, 2013. Despite the fact that the longitudinal separation between STEREO-B and *Wind* is 146°, the summed correlation coefficient for this CIR event is 2.48, which indicates this CIR event can be accurately predicted according to the STEREO-B in-situ observations. We investigate the solar source of this CIR event and discover that the corresponding coronal hole is located across the solar equator. According to Heinemann et al. (2019), the maximal latitudinal southward and northward extents of the coronal hole in the HEEQ coordinate are −0.99° and 13.5°, respectively. It indicates that for a long-lasting CIR event, the spacecraft located 150° trailing Earth in the Solar Ring Mission proposed by (Wang et al., 2020) can also be used to produce a reliable forecast.

From another perspective, Figure 7a compares the number of CIRs that have been accurately predicted by STEREO-B (dark red bars) to all CIRs detected by *Wind* (light red bars) at various longitudinal separation angles. Figure 7b shows the percentage of CIRs that can be accurately forecast (the ratio of CIRs that have been accurately predicted by STEREO-B to the total number of CIRs detected by *Wind*) as a function of longitudinal separations. As illuminated by Figure 7, when the separation angles are less than 40°, only 25% of CIR events are missed by the forecast. The probability of missed CIR events increases with the longitudinal separation angle,

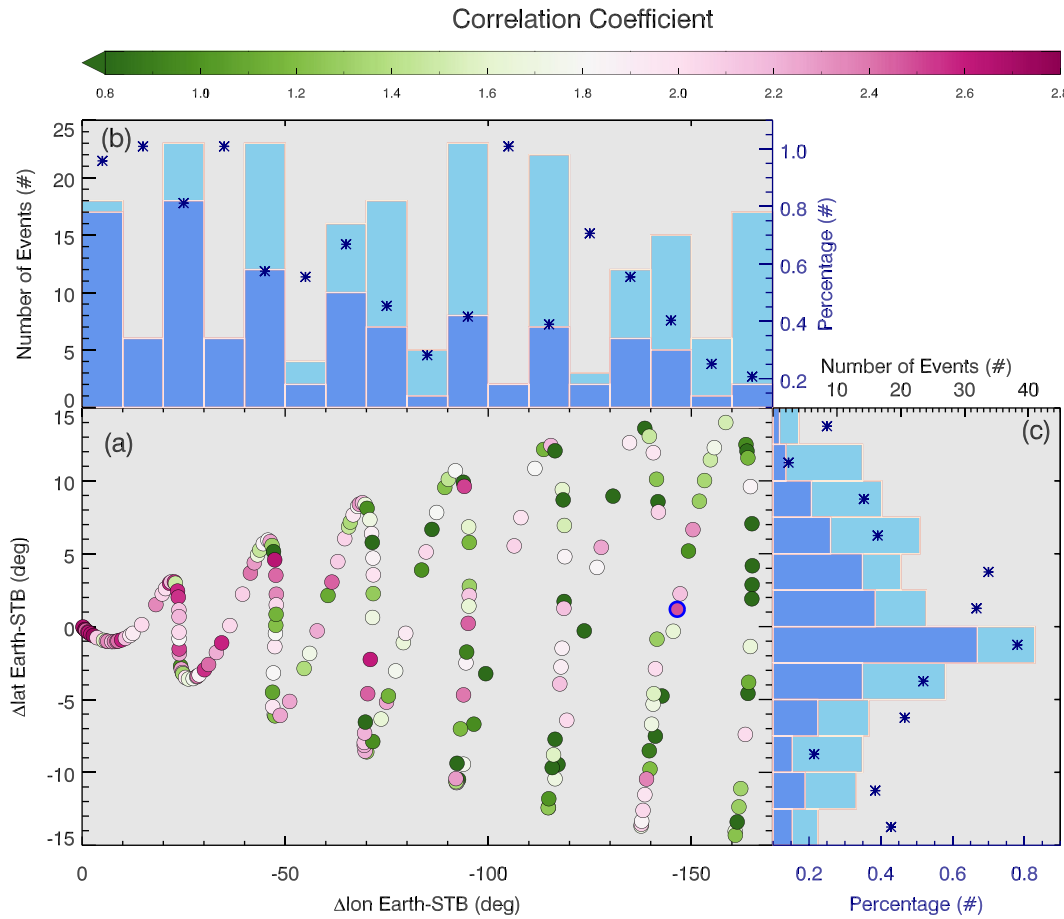

Figure 5. Panel (a) The summed correlation coefficient of corotating interaction regions (CIRs) as a function of different latitudinal and longitudinal separation between time-shifted Solar Terrestrial Relations Observatory (STEREO-B) and *Wind*. Panel (b) Histograms of longitudinal separation angle between STEREO-B and *Wind* spacecraft. Panel (c) Histograms of latitudinal separation angle between STEREO-B and *Wind* spacecraft. The numbers for all CIR occurrences and well-predicted CIR events (summed correlation coefficient more than 1.8) are shown in dark blue and light blue bars, respectively. The blue asterisks represent the likelihood of CIR events that can be predicted accurately.

which is consistent with the findings of the previous study (Allen et al., 2020). When the longitudinal separation angles are larger than 60°, more than a half of CIR events identified at Earth are missed. The significant evolution, diminishing, or disappearance of the coronal hole during the lag time might result in poor prediction. The results indicate that the future solar wind monitor located within 40° longitudinal separation angle can reduce the chance of missing CIRs.

4. Conclusion and Discussion

Using the in-situ data from STEREO-B and *Wind*, we investigate how a solar wind monitor trailing Earth in its orbit can be used to forecast the space weather several days in advance, by analyzing the correlation coefficient of CIRs for magnetic field, velocity, and plasma density. The CIRs detected by STEREO-B (Jian et al., 2018) and *Wind* (Chi et al., 2018; Jian et al., 2006) from 2007 to 2014 are used in this study. During the period of study, the separation longitudinal angle between the STEREO-B and *Wind* increases with time from less than 0.2° to over 165°, while the latitudinal separations fluctuated from −15°to 15°. A total of 219 CIR events recorded by STEREO-B are analyzed in this study after removing those with data gaps or those that interacted with ICMEs. Based on the CIR catalog at STEREO-B, we attempt to find the corresponding CIR events identified by *WIND* according to the correlation coefficient for three key solar wind parameters (magnetic field, velocity, and plasma density). We expect the large-scale CIR structure to remain substantially intact as it moves from STEREO-B

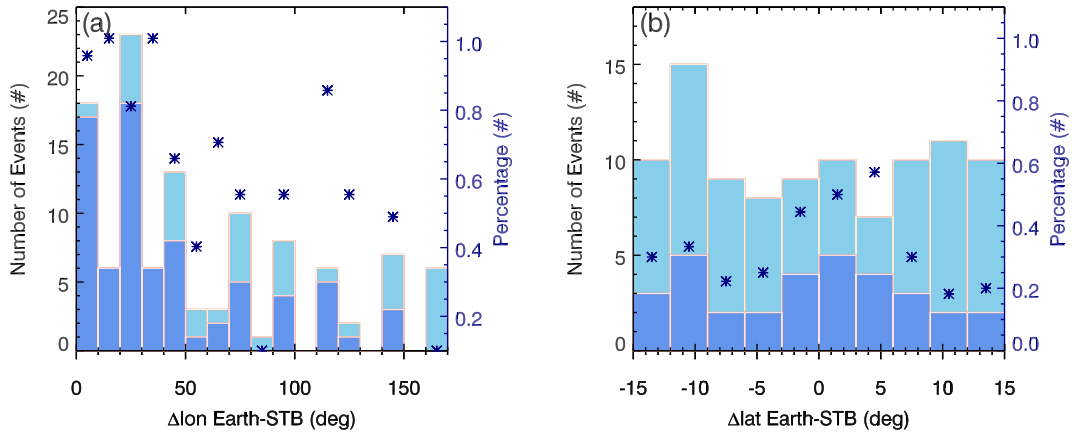

Figure 6. Panel (a) Histograms of longitudinal separation angle between Solar Terrestrial Relations Observatory (STEREO-B) and *Wind* spacecraft for the corotating interaction region (CIR) events with absolute latitude separation less than 5°. Panel (b) Histograms of latitudinal separation angle between STEREO-B and *Wind* spacecraft for the CIR events with longitude separation larger than 90°. The numbers for all CIR events and well-predicted CIR events (summed correlation coefficient more than 1.8) are shown in dark blue and light blue bars, respectively. The blue asterisks represent the likelihood of CIR events that can be predicted accurately.

to Earth when the summed correlation coefficient is more than 1.8. As summarized in Table 1, 58.9% of CIRs detected by STEREO-B can be used to well predict the solar wind condition near-Earth (i.e., with a high correlation between the time series at STEREO and *Wind*). 11.99% of CIR events can find the corresponding CIRs near Earth in the appropriate time window (±30 hr around the benchmark lag time), but with a weak correlation. It is likely because the two CIRs identified by STEREO-B and *Wind* are from different coronal holes, or the coronal hole has undergone significant evolution during the time that the CIR transfer from STEREO-B to Earth. The remaining 29.2% are false alarms. From another point of view, a total of 28.2% CIRs detected by *Wind* according to the catalog from Jian et al. (2006) and Chi et al. (2018) are missed by the forecast from STEREO-B.

We investigate the correlation coefficients between time-shifted STEREO-B and *Wind*, as well as the forecasting capabilities for various longitudinal and latitudinal separation angles. The main findings of this study are summarized as follows:

1. The correlations of magnetic field intensity, solar wind bulk velocity, and plasma density drop rapidly with longitudinal separation angle, indicating that CIR events evolve more significantly as the separation of the two observers increases. The correlation coefficient of the solar wind velocity is significantly higher than the magnetic field and plasma density correlation coefficients, which is consistent with the findings from Miyake et al. (2005).

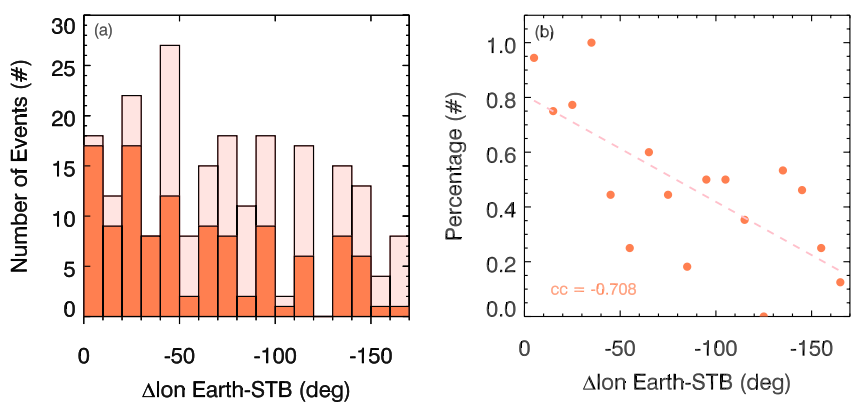

Figure 7. Panel a: Histogram of the longitudinal separation for all the corotating interaction region (CIR) events (light red) and accurately predicted CIR events (dark red). Panel b: shows the percentage of CIRs that can be accurately predicted by Solar Terrestrial Relations Observatory-B in all the CIR events detected by *Wind* spacecraft.

2. The lag time bias has a significant negative correlation with the STEREO-B maximum velocity. It shows that the CIR events with a higher velocity are more likely to arrive at Earth sooner than predicted. The actual lag time is also affected by the relative latitudinal separation angle. Most CIRs will arrive at Earth earlier than predicted when STEREO-B is located to the south of the Earth.
3. The percentage of the accurately predicted CIR events decreases with the longitudinal separation. More than 78% of CIRs can be predicted accurately at the 30° longitudinal separation, which is consistent with the results from Allen et al. (2020). It emphasizes that a future solar wind monitor, such as the Solar Ring Mission (Wang et al., 2020), located 30° trailing Earth in its orbit, may considerably improve the forecasting capabilities of solar wind conditions at Earth. The percentages of accurate prediction drop as the absolute latitudinal separation increase. Within 5° latitudinal separation, more than 66.6% of CIRs can be accurately predicted. It confirms that the latitudinal separation between two observers can affect the accurate prediction of CIRs (M. Owens et al., 2019). When the latitudinal separation is less than 5°, and the longitudinal separation is less than 30°, more than 93.2% CIR events can be well predicted in advance according to STEREO-B in-situ data.

Although, statistical studies show that less than 20.6% of CIRs with longitudinal separations higher than 140° can be accurately predicted. A CIR event detected by STEREO-B on 26–29 November 2013 is found with the summed correlation coefficient of 2.48 when the longitudinal separation is approximately 150° and latitude separation is 1.19°. The high correlation for this event means that the observer at 150° can still provide an advanced warning for the solar wind condition at Earth. A solar wind monitor located at 30° and 150° heliographic longitude ahead of the Sun-Earth line has been proposed by Wang et al. (2020) group, which will hopefully improve the capabilities of our space weather forecasting.

Data Availability Statement

We are grateful to the 1996–2009 ACE/Wind SIR list from from the Appendix in Jian et al. (2006), the 2010–2014 ACE/Wind SIR list from the supplemental information in Chi et al. (2018), and the STEREO SIR catalogue from https://stereo-ssc.nascom.nasa.gov/data/ins_data/impact/level3/SIRs.pdf.

Acknowledgments
We thank the Coordinated Data Analysis Web (CDAWeb) service (http://cdaweb.gsfc.nasa.gov/) for providing *Wind* and STEREO in-situ observations. This work is supported by grants from the Strategic Priority Program of the Chinese Academy of Sciences (XDB41000000), NSFC(41904151, 42004143, 42188101, 42130204), and Anhui Provincial Natural Science Foundation (1908085MD107). We would like to thank the Editor and reviewers for their helpful suggestions to improve the manuscript.

References

Allen, R., Ho, G., Jian, L., Mason, G., Vines, S., & Lario, D. (2020). Predictive capabilities and limitations of stream interaction region observations at different solar longitudes. *Space Weather*, *18*(4), e2019SW002437. https://doi.org/10.1029/2019sw002437

Bagashvili, S. R., Shergelashvili, B. M., Japaridze, D. R., Chargeishvili, B. B., Kosovichev, A. G., Kukhianidze, V., et al. (2017). Statistical properties of coronal hole rotation rates: Are they linked to the solar interior? *Astronomy & Astrophysics*, *603*, A134. https://doi.org/10.1051/0004-6361/201630377

Bailey, R., Möstl, C., Reiss, M., Weiss, A., Amerstorfer, U., Amerstorfer, T., et al. (2020). Prediction of d st during solar minimum using in situ measurements at l5. *Space Weather*, *18*(5), e2019SW002424. https://doi.org/10.1029/2019sw002424

Barnard, L., Owens, M. J., Scott, C. J., Lockwood, M., de Koning, C. A., Amerstorfer, T., et al. (2022). Quantifying the uncertainty in cme kinematics derived from geometric modeling of heliospheric imager data. *Space Weather*, *20*(1), e2021SW002841. https://doi.org/10.1029/2021sw002841

Cannon, P., Angling, M., Barclay, L., Curry, C., Dyer, C., & Edwards, R. (2013). *Extreme space weather: Impacts on engineered systems and infrastructure*. Royal Academy of Engineering.

Chi, Y., Shen, C., Luo, B., Wang, Y., & Xu, M. (2018). Geoeffectiveness of stream interaction regions from 1995 to 2016. *Space Weather*, *16*(12), 1960–1971. https://doi.org/10.1029/2018sw001894

Chi, Y., Shen, C., Wang, Y., Xu, M., Ye, P., & Wang, S. (2016). Statistical study of the interplanetary coronal mass ejections from 1995 to 2015. *Solar Physics*, *291*(8), 2419–2439. https://doi.org/10.1007/s11207-016-0971-5

Echer, E., Tsurutani, B., & Gonzalez, W. (2013). Interplanetary origins of moderate (−100 nt< dst−50 nt) geomagnetic storms during solar cycle 23 (1996–2008). *Journal of Geophysical Research: Space Physics*, *118*(1), 385–392. https://doi.org/10.1029/2012ja018086

Gonzalez, W. D., Echer, E., Tsurutani, B. T., de Gonzalez, A. L. C., & Dal Lago, A. (2011). Interplanetary origin of intense, superintense and extreme geomagnetic storms. *Space Science Reviews*, *158*(1), 69–89. https://doi.org/10.1007/s11214-010-9715-2

Gosling, J., & Pizzo, V. (1999). Formation and evolution of corotating interaction regions and their three dimensional structure. *Corotating interaction regions*, 21–52. https://doi.org/10.1007/978-94-017-1179-1_3

Hapgood, M. (2011). Towards a scientific understanding of the risk from extreme space weather. *Advances in Space Research*, *47*(12), 2059–2072. https://doi.org/10.1016/j.asr.2010.02.007

Harrison, R. G., & Lockwood, M. (2020). Rapid indirect solar responses observed in the lower atmosphere. *Proceedings of the Royal Society A*, *476*(2241), 20200164. https://doi.org/10.1098/rspa.2020.0164

Heinemann, S. G., Temmer, M., Heinemann, N., Dissauer, K., Samara, E., Jerčić, V., et al. (2019). Statistical analysis and catalog of non-polar coronal holes covering the sdo-era using catch. *Solar Physics*, *294*(10), 1–24. https://doi.org/10.1007/s11207-019-1539-y

Jian, L., Luhmann, J., Russell, C., & Galvin, A. (2019). Solar terrestrial relations observatory (stereo) observations of stream interaction regions in 2007–2016: Relationship with heliospheric current sheets, solar cycle variations, and dual observations. *Solar Physics*, *294*(3), 1–27. https://doi.org/10.1007/s11207-019-1416-8

Jian, L., Russell, C., & Luhmann, J. (2011). Comparing solar minimum 23/24 with historical solar wind records at 1 au. *Solar Physics*, *274*(1), 321–344. https://doi.org/10.1007/s11207-011-9737-2

Jian, L., Russell, C., Luhmann, J., & Galvin, A. (2018). Stereo observations of interplanetary coronal mass ejections in 2007–2016. *The Astrophysical Journal*, *855*(2), 114. https://doi.org/10.3847/1538-4357/aab189

Jian, L., Russell, C., Luhmann, J., & Skoug, R. (2006). Properties of stream interactions at one au during 1995–2004. *Solar Physics*, *239*(1), 337–392. https://doi.org/10.1007/s11207-006-0132-3

Kaiser, M. L., Kucera, T., Davila, J., Cyr, O. S., Guhathakurta, M., & Christian, E. (2008). The stereo mission: An introduction. *Space Science Reviews*, *136*(1–4), 5–16. https://doi.org/10.1007/978-0-387-09649-0_2

Luntama, J.-P., Kraft, S., & Glover, A. (2020). Esa Lagrange mission for enhanced space weather monitoring. In *100th American Meteorological Society Annual Meeting*.

Miyake, W., Saito, Y., Hayakawa, H., & Matsuoka, A. (2005). On the correlation of the solar wind observed at the l5 point and at the Earth. *Advances in Space Research*, *36*(12), 2328–2332. https://doi.org/10.1016/j.asr.2004.06.019

Opitz, A., Karrer, R., Wurz, P., Galvin, A. B., Bochsler, P., & Blush, L. (2009). Temporal evolution of the solar wind bulk velocity at solar minimum by correlating the stereo a and b plastic measurements. *Solar Physics*, *256*(1), 365–377. https://doi.org/10.1007/s11207-008-9304-7

Owens, M., Riley, P., Lang, M., & Lockwood, M. (2019). Near-Earth solar wind forecasting using corotation from l5: The error introduced by heliographic latitude offset. *Space Weather*, *17*(7), 1105–1113.

Owens, M. J., Challen, R., Methven, J., Henley, E., & Jackson, D. (2013). A 27 day persistence model of near-Earth solar wind conditions: A long lead-time forecast and a benchmark for dynamical models. *Space Weather*, *11*(5), 225–236. https://doi.org/10.1002/swe.20040

Rodriguez, L., Scolini, C., Mierla, M., Zhukov, A., & West, M. (2020). Space weather monitor at the l5 point: A case study of a cme observed with stereo b. *Space Weather*, *18*(10), e2020SW002533. https://doi.org/10.1029/2020sw002533

Rouillard, A., & Lockwood, M. (2007). Centennial changes in solar activity and the response of galactic cosmic rays. *Advances in Space Research*, *40*(7), 1078–1086. https://doi.org/10.1016/j.asr.2007.02.096

Scott, C., Owens, M., de Koning, C., Barnard, L., Jones, S., & Wilkinson, J. (2019). Using ghost fronts within stereo heliospheric imager data to infer the evolution in longitudinal structure of a coronal mass ejection. *Space Weather*, *17*(4), 539–552. https://doi.org/10.1029/2018sw002093

Scott, C. J., Harrison, R., Owens, M., Lockwood, M., & Barnard, L. (2014). Evidence for solar wind modulation of lightning. *Environmental Research Letters*, *9*(5), 055004. https://doi.org/10.1088/1748-9326/9/5/055004

Simunac, K. D., Kistler, L., Galvin, A., Lee, M., Popecki, M., & Farrugia, C. (2009). In situ observations of solar wind stream interface evolution. *Solar Physics*, *259*(1), 323–344. https://doi.org/10.1007/s11207-009-9393-y

Simunac, K. D., Kistler, L. M., Galvin, A. B., Popecki, M. A., & Farrugia, C. J. (2009). In situ observations from stereo/plastic: A test for l5 space weather monitors. *Annales Geophysicae*, *27*, 3805–3809. https://doi.org/10.5194/angeo-27-3805-2009

Temerin, M., & Li, X. (2002). A new model for the prediction of DST on the basis of the solar wind. *Journal of Geophysical Research*, *107*(A12). SMP–31. https://doi.org/10.1029/2001ja007532

Thomas, S., Fazakerley, A., Wicks, R., & Green, L. (2018). Evaluating the skill of forecasts of the near-Earth solar wind using a space weather monitor at l5. *Space Weather*, *16*(7), 814–828. https://doi.org/10.1029/2018sw001821

Turner, H., Owens, M. J., Lang, M. S., & Gonzi, S. (2021). The influence of spacecraft latitudinal offset on the accuracy of corotation forecasts. *Space Weather*, *19*(8), e2021SW002802. https://doi.org/10.1029/2021sw002802

Vennerstrom, S., Olsen, N., Purucker, M., Acuña, M., & Cain, J. (2003). The magnetic field in the pile-up region at Mars, and its variation with the solar wind. *Geophysical Research Letters*, *30*(7). https://doi.org/10.1029/2003gl016883

Vršnak, B., Dumbović, M., Čalogović, J., Verbanac, G., & Poljanǐć-Beljan, I. (2017). Geomagnetic effects of corotating interaction regions. *Solar Physics*, *292*(9), 1–20.

Wang, Y., Ji, H., Wang, Y., Xia, L., Shen, C., Guo, J., et al. (2020). Concept of the solar ring mission: An overview. *Science China Technological Sciences*, *63*, 1699–1713. https://doi.org/10.1007/s11431-020-1603-2

Wang, Y., Shen, C., Wang, S., & Ye, P. (2003). An empirical formula relating the geomagnetic storm's intensity to the interplanetary parameters:- and δt. *Geophysical Research Letters*, *30*(20). https://doi.org/10.1029/2003gl017901

Yu, B., Scott, C. J., Xue, X., Yue, X., Chi, Y., Dou, X., & Lockwood, M. (2021). A signature of 27 day solar rotation in the concentration of metallic ions within the terrestrial ionosphere. *The Astrophysical Journal*, *916*(2), 106. https://doi.org/10.3847/1538-4357/ac0886